

# A novel continuum damage evolution model based on the concept of damage driving force for unidirectional composites

Tianhong Yu\*, Wenxuan Qi , Elena Sitnikova and Shuguang Li

International Journal of Damage  
Mechanics  
0(0) 1–30

© The Author(s) 2024



Article reuse guidelines:  
sagepub.com/journals-permissions  
DOI: 10.1177/10567895241292744  
journals.sagepub.com/home/ijd



## Abstract

A novel damage evolution model for unidirectional (UD) composites is established in this paper in the context of continuum damage mechanics (CDM). It addresses matrix cracking and it is to be applied along with the damage representation established previously. The concept of damage driving force is employed based on the Helmholtz free energy. It is shown that the damage driving force can be partitioned into three parts, resembling closely three conventional modes of fracture, respectively. A damage evolution law is derived accordingly based on the newly obtained expressions of the damage driving force. The fully rationalised Tsai-Wu criterion is employed in the model for predicting the initiation of matrix cracking damage and fibre failure, assisted with the rationalised maximum stress criterion for identifying the damage modes. A mechanism is introduced to describe the unloading behaviour as a part of the proposed model. The predictions were validated against experimental results, showing good agreement with the experiments and demonstrating the capability and effectiveness of the proposed model.

## Keywords

UD composites, continuum damage mechanics (CDM), matrix cracking, damage driving force, damage evolution, damage initiation

## Introduction

The concept of damage in the field of composites has been widely employed to describe the degradation of effective properties based primarily on the fact that failure of composites is often a process instead of an incident, starting from initiation of micro-cracks to the final rupture.

---

Faculty of Engineering, University of Nottingham, Nottingham, UK

\*Current address: AECC Commercial Aero-Engine Corporation China.

### Corresponding author:

Wenxuan Qi, University of Nottingham, Nottingham, NG7 2RD, UK.  
Email: ezawq2@exmail.nottingham.ac.uk

The continuum damage mechanics (CDM) is one of the approaches to defining the constitutive behaviour associated with damage. The damage is expressed in terms of a state variable so that the constitutive relationship involving damage can be formulated to describe the effects of damage, as opposed to studying individual cracks at a micro-scale, which is not always practical.

Unlike macro-cracks in metallic materials, where a single dominant crack often dictates the eventual failure, micro-cracks in composites are often dispersed in the matrix, sometimes distributed nearly uniformly (Talreja and Singh, 2012). Due to such distribution of micro-cracks, damaged composites can therefore be regarded effectively as a continuum the effective properties of which can be characterised using an appropriate representative volume element, as well as the damage variable introduced to describe the problem of damage. This lays the basis for CDM.

### **Damage representation**

In the framework of CDM, damage models for composite materials normally comprise two major parts, namely, the damage representation and the damage evolution.

Damage representation interprets the physical presence of damage into a mathematical description by utilising a concept of damage variable. With an appropriate definition of the damage variable, the constitutive relationship for the damaged material could be expressed in terms of a relationship amongst stresses, strains and the damage variable.

However, there appeared to be no unique form of damage representation and different forms of constitutive relationships have been obtained as a result. In fact, this issue was exposed in (Allix and Hild, 2002) where it was also argued that some of the forms of suggested constitutive relationships involving damage that may not even be considered as physically or mathematically sound. This situation should be reviewed and improved.

One of the major differences between various damage representation formulations is the way of accounting for the relationship between the degradations of transverse Young's modulus  $E_2$  and in-plane shear modulus  $G_{12}$ . A simple example of such a damage scenario is matrix cracking parallel to fibre direction. This should result in degradations in both transverse modulus  $E_2$  (in tension) and the longitudinal shear modulus ( $G_{12}$ ). The experimental evidence for such damage coupling effect was obtained by Knops and Bögle (Knops and Bögle, 2006), who conducted tests on tubular glass fibre laminate specimens. It was shown that the transverse tensile modulus suffered higher extent of degradation than the in-plane shear modulus.

However, some of the well-known CDM-based damage models for UD lamina employed unrealistic restrictions to interpret this coupled damage effect. In some cases, complete independence between the degradation of  $E_2$  and  $G_{12}$  was assumed (Daghia and Ladeveze, 2013; Matzenmiller et al., 1995; Sapozhnikov and Cheremnykh, 2013; Zinoviev et al., 1998), while in others, identical degradations of  $E_2$  and  $G_{12}$  was imposed (Edge, 1998; Puck and Schürmann, 2002). None of them can be justified physically or mathematically. This issue was also identified during the third World-Wide Failure Exercises (WWFE-III) activities (Kaddour et al., 2013). Moreover, for general 3D stress problems, in presence of matrix cracks parallel to fibres, there will also be coupling between degradations of  $G_{23}$  in addition to that between  $E_2$  and  $G_{12}$ , whilst the effective Poisson's ratios in different directions will be subjected to changes accordingly due to damage.

To address the above problem, some other damage representation models were proposed based on the CDM theory in which the degradation of  $G_{12}$  are determined by the those of  $E_1$  and  $E_2$  (Gupta et al., 2012; Jain and Ghosh, 2009; Mohammadi et al., 2015; Onodera and Okabe, 2020; Salavatian and Smith, 2015; Thollon and Hochard, 2009; Wang et al., 2015; Zhong et al., 2015). Zhong et al (Zhong et al., 2015) proposed a damage representation model for 3D woven composites

including fibre yarns and matrix. In their model, the damage variables representing the damage effects on the shear stiffness of fibre yarns were calculated by the values of the ones characterizing the degradation of longitudinal and transverse modulus. They also considered that the degradation of out-of-plane shear stiffness  $G_{23}$  is determined by the degradation of  $E_2$  and  $E_3$ . Williams et al (Williams et al., 2003) introduced a scalar-valued history parameter to calculate the damage variable and then the residual stiffness functions defined by the damage variables were derived for damage representation.

On the other hand, Li et al. (Li et al., 2019) proposed a damage representation in which the interaction between degradations of  $E_2$  and  $G_{12}$  was accounted for without imposing any artificial restriction, leading to a rational model of damage. It was based on the damage formulation proposed by (Talreja, 1985), who employed a vectorial damage variable. This was a relatively simple damage representation, but it had been proven in (Talreja, 1987) that a more sophisticated tensorial damage variable tended to lead to exactly the same constitutive relationship for matrix cracking damage. By means of virtual experiments and associated mathematical derivations, seven out of eight of these damage-related constants were determined analytically. For the determination of the remaining one, a computational procedure has been developed. As a result, the proposed damage representation (Li et al., 2019) minimised the efforts required for determining damage-related material constants. This damage representation has been adopted in the present paper.

### *Damage initiation criterion and damage evolution law*

Another integral part of the damage model is a damage evolution that describes the growth of damage. Same as for damage representation, different types of damage evolution laws were also proposed by various researchers. These models can be classified into three categories in general, as shown in Table 1.

**Table 1.** Classification of damage evolution laws in damage models for UD lamina.

Damage evolution law types	Damage models
Independent curve-fitting functions derived using direct interpolation of experimental stress-strain curves under specific loading cases, which are not applicable to other loading cases.	A structural-phenomenological model for multi-layered composites under plane stress state by Zinoviev et al. (Zinoviev et al., 1998) A stress-based Grant-Sanders method for predicting failure of composite laminates by Edge (Edge, 1998) Generalized Daniel's model (Daniels, 1945) for fibre-reinforced polymer under a complex loading by Sapozhnikov and Cheremnykh (Sapozhnikov and Cheremnykh, 2013)
Damage evolution laws applicable to general quasi-static loading cases based on the concept of damage surface.	A continuum damage model for modelling transverse matrix cracking damage in composite laminates by Li et al. (Li et al., 1998, 2005). Implementation of the damage theory by Matzenmiller et al. (Matzenmiller et al., 1995) as MAT 162 composite material damage model in LS-DYNA (Haque, 2015; LS-DYNA, 2015). A computational continuum damage mechanics model for notched cross-ply composite laminates by Babaei et al (Babaei and Farrokhabadi, 2017)
Damage evolution laws applicable to general loading cases based on damage driving force.	Enhanced meso-model for laminated composites by Ladeveze and Daghia (Daghia and Ladeveze, 2013).

Apart from the aforementioned models, other researchers proposed numerical methods to address the mechanical properties and cracking problems in UD composites (Galadima et al., 2023), including the extended finite element method (XFEM) (Abdullah et al., 2017; Dimitri et al., 2017; Swati et al., 2019), peridynamics (PD) model (Li et al., 2023; Ni et al., 2023; Sun et al., 2023), lattice model (Braun and Ariza, 2020; Braun et al., 2021, 2024) and so on. Li et al. (Li et al., 2023) proposed a highly efficient bond-based PD model to simulate the progressive damage behaviour of laminated composites. In their model, critical values and damage characteristics for different damage modes at material points were defined to predict the evolution of damage in composite structures. Braun et al. (Braun and Ariza, 2020) presented an extended linear elastic lattice model for anisotropic materials. A softening constitutive law in terms of an equivalent displacement was introduced in the model to predict the progressive damage evolution in composite materials. Mukhopadhyay et al. (Mukhopadhyay and Hallett, 2019) presented a new direct CDM model for matrix cracking in composites and it is implemented using Abaqus. A damage variable was introduced in the bilinear damage evolution law based on the calculated mixed-mode critical energy release rate. In their model, the fibre orientation at ply level was also used as an input so that individual matrix cracks in cracked plies could be represented and their evolution could be tracked, making their model independent of mesh pattern.

The objective of this paper is to supplement the damage representation formulated in (Li et al., 2019) for matrix cracking damage in UD composites with a novel damage evolution law based on the concept of damage driving force. Whilst retaining the necessary consistency in its formulation, a great simplification will be brought forward by some rigorous mathematical transformation in the presentation of the damage driving force, resulting in three naturally partitioned components directly associated with the corresponding stress components, resembling the conventional fracture modes.

In absence of pre-existing defects or damage, a damage initiation criterion is usually required to trigger the onset of damage process, therefore a complete formulation of the damage model should be supplemented by a damage initiation condition. Failure criteria for UD composites are often employed as the damage initiation criteria, and their comprehensive reviews can be found from the outcomes of WWFEs (Hinton et al., 2002, 2004; Kaddour and Hinton, 2013; Kaddour et al., 2004, 2013; Soden et al., 1998, 2004) and (Echaabi et al., 1996). The recently fully rationalised Tsai-Wu criterion (Li et al., 2022a, 2022b) will be employed for damage onset, assisted with the rationalised maximum stress criterion (Li, 2020) for the identification of the damage mode. The predicted damage initiation has also been compared with that obtained using the Puck criterion (Knops, 2008) in terms of damage initiation and its knock-on effects on the subsequent damage process.

In addition to predicting the onset of the transverse matrix cracking damage in laminated composites under quasi-static loading, the failure criterion employed can also help with the prediction of catastrophic failure modes like fibre failures. The model has been formulated in such a way that it is applicable to general loading conditions including unloading and reloading scenarios, a mechanism not present in many existing damage models, yet crucial in representing the effective of irreversible nature of a damage process. Finally, the predicted results will be compared to experimental data from quasi-static tests on composite laminates to validate the model developed.

## **Damage representation for matrix cracking in UD composites**

The damage representation established by Li et al. (Li et al., 2019) is adopted in this paper to incorporate the effects of damage in the form of matrix cracks on the elastic behaviour of UD



### Damage initiation criterion

Built on top of the knowledge acquired through the World-Wide Failure Exercises (WWFEs) (Hinton et al., 2002; Kaddour and Hinton, 2012; Kaddour et al., 2013a, 2013b), two most popular criteria, *viz.* the maximum stress criterion and the Tsai-Wu criterion have been fully rationalised recently (Li, 2020; Li et al., 2022a, 2022b). Together, they can offer a complete damage initiation criterion, with the rationalised Tsai-Wu criterion for the damage onset and the rationalised maximum stress criterion for the crack orientation as the damage mode.

The rationalised Tsai-Wu criterion for UD composites under a general 3D stress state can be given as follows (Li et al., 2022a, 2022b)

$$F_1\sigma_1 + F_2(\sigma_2 + \sigma_3) + F_{11}\sigma_1^2 + F_{22}(\sigma_2^2 + \sigma_3^2 - \sigma_2\sigma_3 + 3\tau_{23}^2) - \sqrt{F_{11}F_{22}}\sigma_1(\sigma_3 + \sigma_2) + F_{66}(\tau_{13}^2 + \tau_{12}^2) = 1 \quad (4)$$

where

$$F_1 = \frac{1}{X_t} - \frac{1}{X_c}, F_2 = \frac{1}{Y_t} - \frac{1}{Y_c}, F_{11} = \frac{1}{X_t X_c}, F_{22} = \frac{1}{Y_t Y_c} \text{ and } F_{66} = \frac{1}{S_L^2} \quad (5)$$

with  $X_t$ ,  $X_c$ ,  $Y_t$ ,  $Y_c$  and  $S_L$  being the tensile and compressive strengths along and transverse to the fibres and the shear strength along fibres, respectively. One of the logical outcomes of the rationalisation made to the Tsai-Wu criterion was that in it, the transverse shear strength is a derived property and hence its value does not need to be specified explicitly. Given the linear elastic response prior to damage initiation, the onset point can be determined by a load factor as

$$\lambda = \frac{-L + \sqrt{L^2 + 4Q}}{2Q} \quad (6)$$

where

$$L = F_1\sigma_1 + F_2(\sigma_2 + \sigma_3)$$

$$Q = F_{11}\sigma_1^2 + F_{22}(\sigma_2^2 + \sigma_3^2) - F_{22}\sigma_2\sigma_3 - \sqrt{F_{11}F_{22}}\sigma_1(\sigma_3 + \sigma_2) + 3F_{22}\tau_{23}^2 + F_{66}(\tau_{13}^2 + \tau_{12}^2) \quad (7)$$

The maximum stress criterion was rationalised primarily in the plane transverse to fibres (Li, 2020), in the sense that failure transverse to fibres should be determined by

$$\left\{ \begin{array}{l} \sigma_{II}^M \\ \sigma_{III}^M \end{array} \right\} = \frac{\sigma_2 + \sigma_3}{2} \pm \sqrt{\tau_{23}^2 + \left( \frac{\sigma_2 - \sigma_3}{2} \right)^2} \quad (8)$$

where  $\sigma_{II}^M$  and  $\sigma_{III}^M$  are direct stress transverse to fibres with superscript  $M$  signifying that  $\sigma_{II}^M$  is the maximum tensile stress if  $\sigma_{II}^M \geq 0$  and/or  $\sigma_{III}^M$  the maximum compressive stress if  $\sigma_{III}^M < 0$ . Although the expression of  $\sigma_{II}^M$  and  $\sigma_{III}^M$  are identical to those of the principal stresses under a 2D stress state,

they are not principal stresses as the current stress state in 3D and on the plane where these stress are found, the shear stress in the direction along fibres does not vanish, in general.

As illustrated in Figure 1(a), the transverse failure plane in UD composites is always parallel to the fibre direction. Under transverse loading, from the equilibrium conditions for the free body diagram as illustrated in Figure 1(b), the following two equations can be obtained

$$\begin{aligned}\sigma_3 \sin \theta + \tau_{23} \cos \theta &= \sigma_M \sin \theta \\ \sigma_2 \cos \theta + \tau_{23} \sin \theta &= \sigma_M \cos \theta\end{aligned}\quad (9)$$

where  $\sigma_M$  and  $\theta$  denoting the maximum direct stress and the angle of maximum direct stress and the axis 2, respectively.

By combining the above two equations and eliminating  $\sigma_M$ , the angle between the maximum direct stress and the coordinate axis 2 is given as

$$\theta = \frac{1}{2} \tan^{-1} \frac{2\tau_{23}}{\sigma_2 - \sigma_3} \quad \text{where} \quad -\frac{\pi}{2} \leq \theta \leq \frac{\pi}{2}\quad (10)$$

Under uniaxial transverse tension, the normal to the failure plane is identical to the direction of the applied tensile stress  $\sigma_M$  according to the rationalised maximum stress criterion (Li, 2020), on which the shear stress is equal to zero. One has  $\theta_t = \theta = 0$ .

Under a uniaxial transverse compression stress condition (when  $\tau_{23} = 0$ ), the failure is primarily due to the transverse shear stress on the fracture plane. According to the Mohr's circle, the maximum shear stress is found on a plane  $\pm\pi/4$  from the direction of applied compressive stress (also  $\pm\pi/4$  from the direction of  $\sigma_M$  which is 0 in magnitude in this case). As  $\theta$  is equal to 0, the angle between the failure plane and axis 2 can be obtained as

$$\theta_c = \pm \frac{\pi}{4} + \theta = \pm \frac{\pi}{4}\quad (11)$$

The experimental result is obtained as  $56.5^\circ$ , and a commonly-used test value is  $53^\circ$  (Tao et al., 2017). Besides, the Puck criterion (Knops, 2008) also predicted an angle slightly different from  $\pm\pi/4$ .

The longitudinal shear failure is determined by the maximum longitudinal shear stress

$$\tau_L = \sqrt{\tau_{12}^2 + \tau_{13}^2}\quad (12)$$

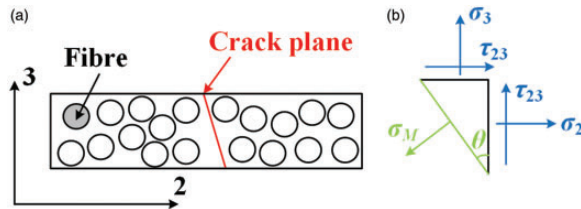


**Figure 1.** Illustration of transverse failure plane in UD composites.

instead of any individual longitudinal shear stress on a coordinate plane. The normal to the failure plane is at an angle

$$\theta_s = \tan^{-1} \frac{\tau_{12}}{\tau_{13}} \text{ where } -\frac{\pi}{2} \leq \theta_s \leq \frac{\pi}{2} \quad (13)$$

to the coordinate axis 2.

Once damage onset is predicted by the rationalised Tsai-Wu criterion, the following ratios will be examined

$$\frac{\sigma_1}{X_t} \text{ (if } s_1 \text{ is positive), } \frac{|\sigma_1|}{X_c} \text{ (if } s_1 \text{ is negative)} \quad (14)$$

$$\frac{\sigma_{II}^M}{Y_t} \text{ (if } \sigma_{II}^M \text{ is positive), } \frac{|\sigma_{III}^M|}{Y_c} \text{ (if } \sigma_{III}^M \text{ is negative) and } \frac{\tau_L}{S_L} \quad (15)$$

and the highest will dictate the failure mode. Predictions dictated by (14) in fibre mode will usually lead to catastrophic failure of the structure and damage modelling is not relevant. Those predicted by any in (15) are matrix dominated and characterised by some kind of matrix cracks parallel to fibres as illustrated in Figure 2, where the crack orientation can be determined as from (10), (11) or (13) depending on the dictating ratio from (15).

### The damage evolution model

Having introduced the damage initiation criterion, a novel damage evolution law is proposed below to describe the evolution of matrix cracking under general quasi-static loading.

*Derivation of damage driving force.* To be consistent with the damage representation derived from the Helmholtz free energy density, it is natural to derive the corresponding damage evolution law based on the concept of damage driving force from the same energy as well, offering a natural connection in the theoretical framework between damage representation and damage evolution.

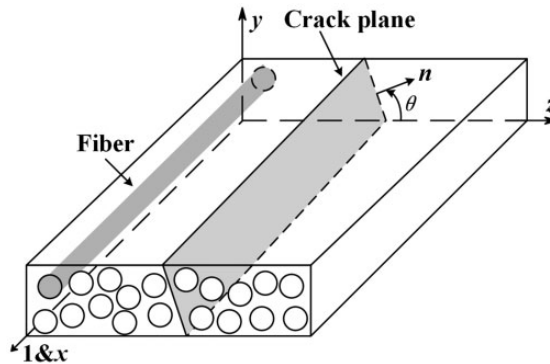


**Figure 2.** UD composite matrix cracking damage orientation definition.

For vector field characterization of damage in composites, a damage vector  $V = [v_1 \ v_2 \ v_3]^T$  defined in (Li et al., 2019; Talreja, 1985) was introduced, which is shown as follow,

$$\mathbf{V}^{(\alpha)} = D^{(\alpha)} \mathbf{n}^{(\alpha)}, \quad \alpha = 1, 2, 3 \quad (16)$$

where  $D^{(\alpha)}$  is a suitably defined average over the volume, and  $\mathbf{n}^{(\alpha)}$  is a unit vector normal to the crack planes whose direction is parallel to the  $\alpha$  axis. Then the Helmholtz free energy density can be expanded into a Taylor series. Its expression in terms of irreducible invariant integrity bases had been presented in (Li et al., 2019) for UD composites. Since the first order terms are associated with the initial stresses and the initial damage, they can be waived if such effects are not present in the problem under consideration. On the other hand, all terms higher than the second order are deemed to be high order terms. The formulation can therefore be truncated at the second order terms of strains and damage for problems involving small deformation and small damage. In the formulation in (Matzenmiller et al., 1995), the terms involving second order of damage were also dropped because they did not contribute to stresses in the damage representation. However, they will contribute to the damage driving force and therefore should be retained for the formulation of the damage evolutionary law. As a result, the Helmholtz free energy density  $\Psi$  can be expressed as

$$\Psi = \frac{1}{2} \left( \begin{array}{l} A_1 I_1^2 + A_2 I_1 I_2 + A_3 I_1^2 I_5^2 + A_4 I_1 I_5 I_6 + A_5 I_1^2 I_8 + A_6 I_1 I_9 + A_7 I_1 I_2 I_5^2 \\ + A_8 I_1 I_2 I_8 + B_1 I_2^2 + B_2 I_2^2 I_5^2 + B_3 I_2 I_5 I_6 + B_4 I_2^2 I_8 + B_5 I_2 I_9 + C_1 I_3 \\ + C_2 I_3 I_5^2 + C_3 I_3 I_8 + D_1 I_4 + D_2 I_4 I_5^2 + D_3 I_4 I_8 + E_1 I_5 I_7 + F_1 I_6^2 \\ + G_1 I_5^2 + G_2 I_8 \end{array} \right) + O_2(\varepsilon, V) \quad (17)$$

where the irreducible integrity bases are defined as

$$\begin{aligned} I_1 &= \varepsilon_1 \\ I_2 &= \varepsilon_2 + \varepsilon_3 \\ I_3 &= 2\varepsilon_2^2 + \gamma_{23}^2 + 2\varepsilon_3^2 \\ I_4 &= \gamma_{13}^2 + \gamma_{12}^2 \\ I_5 &= v_1 \\ I_6 &= v_2 \gamma_{12} + v_3 \gamma_{13} \\ I_7 &= 2v_2 \varepsilon_2 \gamma_{12} + v_2 \gamma_{23} \gamma_{13} + v_3 \gamma_{23} \gamma_{12} + 2v_3 \varepsilon_3 \gamma_{13} \\ I_8 &= v_2^2 + v_3^2 \\ I_9 &= v_2^2 \varepsilon_2 + v_2 v_3 \gamma_{23} + v_3^2 \varepsilon_3. \end{aligned} \quad (18)$$

where  $v_i$  are components of the damage vector as originally defined in (Li et al., 2019) (be aware of the disparity between letter vee,  $v$ , in Norman face to distinguish from Greek nu,  $\nu$ , for the Poisson's ratios),  $\varepsilon_1$ ,  $\varepsilon_2$  and  $\varepsilon_3$  are direct strains and  $\gamma_{23}$ ,  $\gamma_{13}$  and  $\gamma_{12}$  engineering shear strains. In comparison with the Helmholtz free energy density employed in (Li et al., 2019), there are two additional terms involving damage variable only associated with coefficients  $G_1$  and  $G_2$ , respectively. Coefficients  $A_1 \sim A_8$ ,  $B_1 \sim B_5$ ,  $C_1 \sim C_3$ ,  $D_1 \sim D_3$ ,  $E_1$  and  $F_1$  are the constants associated with the effective stiffness matrix of the damaged composite and they were all as involved in (Li et al., 2019). With the Helmholtz free energy density expression as given in (16), the components of the damage driving force can be obtained as

$$R_i = -\frac{\partial \Psi}{\partial v_i} \quad (i = 1, 2, 3) \quad (19)$$

It should be noted that since energy is being released from the material during a cracking process, negative sign is introduced here to reflect this negative gain. The damage driving force can be expressed in general as follows

$$\begin{Bmatrix} R_1 \\ R_2 \\ R_3 \end{Bmatrix} = \begin{bmatrix} W_{11} & W_{12} & W_{13} \\ W_{21} & W_{22} & W_{23} \\ W_{31} & W_{32} & W_{33} \end{bmatrix} \begin{Bmatrix} v_1 \\ v_2 \\ v_3 \end{Bmatrix} \quad (20)$$

where  $W_{ij}$  ( $i, j = 1, 2, 3$ ) are quadratic expressions of strains.

Referring to Figure 2, the local coordinate system can be so chosen that the damage vector  $V = [v_1 \ v_2 \ v_3]^T$  is aligned with  $\mathbf{n}$ , the normal to the cracks, so that the damage vector will always be  $V = [0 \ v_2 \ 0]^T$ , as was the case in (Li et al., 2019), where a single array of microcracks is present within the representative volume of the material. The new coordinate system is shown in Figure 3. Thus, the damage representation as given in (1) and (2) can be employed directly. In the case where the local coordinate system of material differs from that defined above, a conventional coordinate transformation would suffice to reconcile the differences in the obtained expressions of the effective stiffness matrices due to the use of different coordinate systems.

Assume that as the damage evolves, microcracks keep their orientation, as is usually the case in the most popular scenarios of transverse matrix cracking in laminated composites. In other words,  $R_1$  and  $R_3$  would not make any difference as there is no relevant damage components for them to drive, no matter how significant their values become. Component  $R_2$  will be the only one having effects on the damage evolution. Given  $v_1 = v_3 = 0$ , one has

$$R_2 = W_{22}v_2 \quad (21)$$

where

$$W_{22} = \{\varepsilon\}^T [\mathbf{Y}] \{\varepsilon\} + G_2 \quad (22)$$

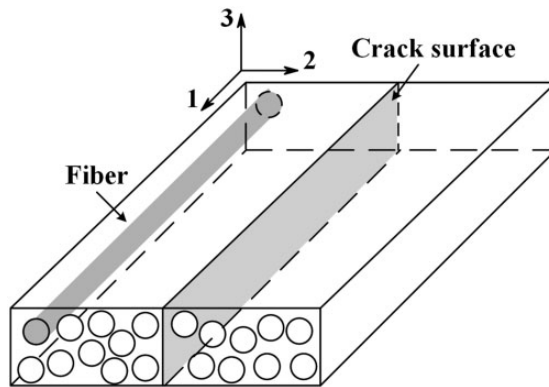


**Figure 3.** Rectangular material coordinate system assigned to UD composites.

with

$$[\mathbf{Y}] = \begin{bmatrix} 2A_5 & A_6 + A_8 & A_8 & 0 & 0 & 0 \\ A_6 + A_8 & 2B_4 + 2B_5 + 4C_3 & 2B_4 + B_5 & 0 & 0 & 0 \\ A_8 & 2B_4 + B_5 & 2B_4 + 4C_3 & 0 & 0 & 0 \\ 0 & 0 & 0 & 2C_3 & 0 & 0 \\ 0 & 0 & 0 & 0 & 2D_3 & 0 \\ 0 & 0 & 0 & 0 & 0 & 2F_1 + 2D_3 \end{bmatrix} \quad (23)$$

Before the material undergoes any deformation,  $G_2$  would be the only non-vanishing term in  $W_{22}$ , implying the presence of damage driving force  $R_i$  even then, provided that damage  $v_i$  is not zero. The same argument also applies to the constant term of  $G_1$  in  $W_{11}$ . Obviously, such a scenario corresponds to a case in presence of initial damage in the material. For simplicity,  $G_1$  and  $G_2$  are set to zero, implying the absence of initial damage for the subsequent development in this paper.

Recall the relationship between damage vector component  $v_2$  and damage parameter  $\omega$  in (Li et al., 2019),

$$\omega = \lambda v_2^2 \text{ with } \omega = \frac{E_2^0 - E_2}{E_2^0} \quad (24)$$

where  $\lambda$  is a proportion factor between damage parameter  $\omega$  which has a definitive measure of magnitude as the relative change in the effective transverse modulus and the vectorial damage variable which is defined through the surface area of microcracks. Factor  $\lambda$  will eventually disappear as in (Li et al., 2019) when damage variable  $v$  is subsequent replaced by damage parameter  $\omega$ , for the specific type of damage as is dealt with in this paper, as well as in (Li et al., 2019). To drive the damage expressed in terms of  $\omega$ , it is appropriate to redefined the damage driving force with respect to  $\omega$  and denoted as  $\rho$

$$\rho = -\frac{\partial \psi}{\partial \omega} = -\frac{\partial \psi}{\partial v_2} \frac{\partial v_2}{\partial \omega} = -\frac{W_{22}}{2\lambda} = -\frac{1}{2\lambda} \{\varepsilon\}^T [\mathbf{Y}] \{\varepsilon\} \quad (25)$$

where  $[\mathbf{Y}]$  is defined in (23). Expressing the strains in terms of stresses using the strain-stress relationship in presence of damage, i.e., the inverse of (3), the expression of  $\rho$  as in (25) can be re-written as

$$\rho = -\frac{1}{2\lambda} \{\boldsymbol{\sigma}\}^T [\mathbf{S}]^T [\mathbf{Y}] [\mathbf{S}] \{\boldsymbol{\sigma}\} = \{\boldsymbol{\sigma}\}^T [\mathbf{P}] \{\boldsymbol{\sigma}\} \quad (26)$$

where  $[\mathbf{S}]$  is the inverse of  $[\mathbf{C}]$  as given in (1). As a result of this simple yet rigorous mathematical transformation, a very attractive presentation of  $[\mathbf{P}]$  is obtained as

$$[\mathbf{P}] = -\frac{1}{2\lambda} [\mathbf{S}]^T [\mathbf{Y}] [\mathbf{S}] = \begin{bmatrix} 0 & 0 & 0 & 0 & 0 & 0 \\ & P_I & 0 & 0 & 0 & 0 \\ & & 0 & 0 & 0 & 0 \\ & & & P_{III} & 0 & 0 \\ & & & & 0 & 0 \\ & & & & & P_{II} \end{bmatrix} \quad (27)$$

After linearization with respect to  $\omega$  under the assumption of small damage, i.e.,  $\omega \ll 1$ , one obtains

$$\begin{aligned} P_I &= P_I^0 + P_I^D \omega \\ P_{II} &= P_{II}^0 + P_{II}^D \omega \\ P_{III} &= P_{III}^0 + P_{III}^D \omega \end{aligned} \quad (28)$$

where

$$\begin{aligned} P_I^0 &= \frac{1}{E_2^0}, & P_I^D &= \frac{2(1 - \nu_{12}^0 \nu_{21}^0)}{(1 - \nu_{23}^0 - 2\nu_{12}^0 \nu_{21}^0)(1 + \nu_{23}^0)E_2^0} \\ P_{II}^0 &= \frac{k}{G_{12}^0}, & P_{II}^D &= \frac{2k^2}{G_{12}^0} \\ P_{III}^0 &= \frac{1}{E_2^0}, & P_{III}^D &= \frac{1}{(1 + \nu_{23}^0)E_2^0} \end{aligned} \quad (29)$$

with  $k$  being the same as that in (2). It can be noted that the proportion factor  $\lambda$  has disappeared from the expression of  $[\mathbf{P}]$  as expected.

As a result, the damage driving force  $\rho$  in (25) for the specific form of damage, i.e., matrix cracking, can be expressed as

$$\rho = \rho_I + \rho_{II} + \rho_{III} \quad \text{with} \quad \begin{aligned} \rho_I &= P_I \sigma_2^2 \\ \rho_{II} &= P_{II} \tau_{12}^2 \\ \rho_{III} &= P_{III} \tau_{23}^2 \end{aligned} \quad (30)$$

where each of the three parts is directly associated with transverse direct stress  $\sigma_2$ , longitudinal shear stress  $\tau_{12}$  and transverse shear stress  $\tau_{23}$ , in a completely decoupled manner.

As shown in equation (27), there are only three non-zero elements in matrix  $[P]$ , and they dictate the damage driving force  $\rho$ . Expressions (27) to (29) were rigorously derived analytically, although use was made of mathematical software Maple (Maplesoft, 2014) to ease the mathematical manipulations. The sparse appearance of  $[\mathbf{P}]$  and the explicit decoupled expression of the damage driving force  $\rho$  as given in (30) are apparently of great simplicity. They are naturally linked to the three conventional modes of fracture. The subscripts *I*, *II* and *III* introduced in (27) for  $P$  terms and in (30) for  $\rho$  terms represent the corresponding modes when the microcracks are viewed from the direction of axis 3. Different from fracture modes in conventional fracture mechanics which are associated with a specific crack, the modes here characterise the damaged material as a whole.

The expression of the damage driving force derived above and the damage representation previously established in (Li et al., 2019) are fully consistent. Assisted with the damage initiation criterion and the identification of the damage mode as proposed in Section ‘Damage initiation criterion’, a novel and complete matrix cracking damage model has been formulated.

From (28), (29) and (30), it can be seen that the newly derived damage driving force  $\rho$  can be expressed explicitly in terms of the effective elastic constants of the undamaged UD composites, the damage parameter and stresses, without introducing any new constants as fudge factors, and its physical dimension is the same as stresses. In this case, under a loading condition in which stresses increase monotonically, damage driving force  $\rho$  would increase accordingly according to (30). In

such a loading process from a stress-free initial state, the damage evolution process is triggered when the damage initiation criterion is satisfied.

If  $\rho$  is regarded as the total damage driving force, it consists of three parts as naturally partitioned in (30). Similar to the concept of mixed mode fracture, the three parts of the damage driving force should be counted independently in order to form a damage growth law in a mixed mode sense as is the subject of the next subsection.

*Critical damage driving forces and a mixed mode damage growth law.* The total damage driving force  $\rho$  as obtained above is apparently not completely determined by the material properties. It is also affected by the loading conditions, i.e., different stress ratios. This is similar to the observation in fracture mechanics where critical total energy release rate is not a material property but varies with the mode ratio. It has to be partitioned into individual modes and compared with their respective critical values,  $G_{Ic}$ ,  $G_{IIc}$  and  $G_{IIIc}$ , before the mixed mode problem can be meaningfully addressed (Anderson, 2017). The same argument applies to the total damage driving force. Critical values as material properties will have to be associated with individual modes, i.e.,  $\rho_{Ic}$ ,  $\rho_{IIc}$  and  $\rho_{IIIc}$ . Each of these critical damage driving forces has to be obtained under a single mode of loading right up to the point of damage growth as follows:

$$\begin{aligned}\rho_{Ic} &= P_I \sigma_{2c}^2 \\ \rho_{IIc} &= P_{II} \tau_{12c}^2 \\ \rho_{IIIc} &= P_{III} \tau_{23c}^2\end{aligned}\quad (31)$$

where  $\sigma_{2c}$ ,  $\tau_{12c}$  and  $\tau_{23c}$  are uniaxial or pure shear stress threshold values for damage growth initiation at the current damage state. They can vary with the damage variable  $\omega$  in general. However, as a first approximation, they are assumed to be constant and hence material properties. Their values can therefore be evaluated at  $\omega = 0$ , i.e.

$$\begin{aligned}\rho_{Ic} &= P_I^0 \sigma_{2c}^2 \\ \rho_{IIc} &= P_{II}^0 \tau_{12c}^2 \\ \rho_{IIIc} &= P_{III}^0 \tau_{23c}^2\end{aligned}\quad (32)$$

where superscript ‘0’ indicates the corresponding values obtained at  $\omega = 0$ . According to equations (29) and (32), it can be seen that the critical damage driving forces can be considered as threshold values of the critical total potential energy release rate with respect to damage. The critical damage driving forces are also adopted to define the criteria of unloading and reloading process when analysing the damage evolution in composite materials under complex loading conditions, as will be demonstrated in Section ‘Unloading and reloading scenarios’.

Based on above discussion, the total damage driving force  $\rho$  is divided into three parts, which represent corresponding individual modes respectively for mixed-mode loading cases. Some kind of mixed mode damage evolution law will have to be resorted to as in the case of mixed mode fracture. Let

$$\eta = \left(\frac{\rho_I}{\rho_{Ic}}\right)^\alpha + \left(\frac{\rho_{II}}{\rho_{IIc}}\right)^\beta + \left(\frac{\rho_{III}}{\rho_{IIIc}}\right)^\gamma \quad (33)$$

where  $\eta$  represents the combined equivalent effect from all pure mode damage driving forces so that mixed-mode loading condition can be accounted for. The critical condition for damage to evolve is

$$\eta = 1 \quad (34)$$

Although constants  $\alpha$ ,  $\beta$  and  $\gamma$  could each take different values and should be determined by fitting available experimental data to achieve a best fit, the lack of sufficient experimental data renders a fairly arbitrarily selected value of  $\alpha = \beta = \gamma = 1$  or 2 as a practical approximation as is also case in the practices of mixed mode fracture mechanics (Anderson, 2017).

*Damage evolution law and incremental material constitutive relationship.* From the derivation of damage driving force, the quantities driving the evolution of damage have been clearly identified, and they determine whether the damage will grow. However, an additional relationship is required between the damage driving force and the amount of damage growth.

For this, an incremental relationship is presented as follows. Since damage growth is driven by damage driving force, it is then conceivable that the magnitude of damage should be a function of the three independent components of the damage driving force, i.e.

$$\omega = f(\rho_I, \rho_{II}, \rho_{III}) \quad (35)$$

Imagine the critical state for damage initiation is met once the values of the damage driving force components reach  $\rho_{I0}$ ,  $\rho_{II0}$  and  $\rho_{III0}$  at a given damage level  $\omega_0$ . One can expand the function in (35) into a Taylor's series in the neighbourhood of the state. Neglecting terms of orders higher than the first, the following equation is obtained,

$$\omega \approx \omega_0 + \mu_I(\rho_I - \rho_{I0}) + \mu_{II}(\rho_{II} - \rho_{II0}) + \mu_{III}(\rho_{III} - \rho_{III0}) \quad (36)$$

where  $\mu_I$ ,  $\mu_{II}$  and  $\mu_{III}$  are damage-evolution-related constants which are material properties and should be determined based on experimental data. Equation (36) can be expressed in an alternative manner as

$$\Delta\omega = \mu_I\Delta\rho_I + \mu_{II}\Delta\rho_{II} + \mu_{III}\Delta\rho_{III} \quad (37)$$

This is the incremental relationship between the damage and the components of the damage driving force. In general, damage-evolution-related constants for a given material system,  $\mu_I$ ,  $\mu_{II}$  and  $\mu_{III}$  in (37), correspond to each of the three different modes and therefore take different values, implying that loads in different modes make different contributions to damage growth.

It also can be seen from (37) that the damage evolves only when the components of the damage driving force produce a positive value for  $\Delta\omega$ . Otherwise, unloading takes place, as will be addressed in the next subsection.

According to the continuum damage mechanics, the second law of continuum thermodynamics leads to the following Clausius-Duhem inequality (Murakami, 2012),

$$\boldsymbol{\sigma} : \dot{\boldsymbol{\varepsilon}}^p + \rho\dot{\omega} + (\mathbf{g}/T) \cdot \mathbf{q} \geq 0 \quad (38)$$

where  $\boldsymbol{\sigma}$  and  $\boldsymbol{\varepsilon}^p$  denoting the stress and plastic strain, respectively;  $\omega$  and  $\rho$  denoting the damage variable and the associated damage driving force, respectively;  $\mathbf{g}$  and  $\mathbf{q}$  being temperature gradient and heat flux vector, respectively, and  $T$  being the temperature.

In our model, the inelastic strain is not considered, and a uniform temperature field is assumed. So, the above inequality leads to the following condition,

$$\rho \dot{\omega} \geq 0 \quad (39)$$

Hence, satisfying the above inequality will ensure our proposed damage evolution law thermodynamically admissible. This inequality imposes restrictions on the values of damage-evolution-related constants  $\mu_I$ ,  $\mu_{II}$  and  $\mu_{III}$  such that the incremental damage value  $\Delta\omega$  predicted by (37) should always satisfy (39) after (39) is approximated by its incremental form instead of rate form.

The incremental form of  $\rho_I$ ,  $\rho_{II}$  and  $\rho_{III}$  can be given as

$$\begin{aligned} \Delta\rho_I &= \left( P_I^0 + P_I^D(\omega_0 + \Delta\omega) \right) (\sigma_2 + \Delta\sigma_2)^2 - (P_I^0 + P_I^D\omega_0)\sigma_2^2 \\ \Delta\rho_{II} &= \left( P_{II}^0 + P_{II}^D(\omega_0 + \Delta\omega) \right) (\tau_{12} + \Delta\tau_{12})^2 - (P_{II}^0 + P_{II}^D\omega_0)\tau_{12}^2 \\ \Delta\rho_{III} &= \left( P_{III}^0 + P_{III}^D(\omega_0 + \Delta\omega) \right) (\tau_{23} + \Delta\tau_{23})^2 - (P_{III}^0 + P_{III}^D\omega_0)\tau_{23}^2 \end{aligned} \quad (40)$$

Substituting them into (37) yields

$$\begin{aligned} \Delta\omega &= \mu_I \left\{ [P_I^0 + P_I^D(\omega_0 + \Delta\omega)] (\sigma_2 + \Delta\sigma_2)^2 - (P_I^0 + P_I^D\omega_0)\sigma_2^2 \right\} \\ &\quad + \mu_{II} \left\{ [P_{II}^0 + P_{II}^D(\omega_0 + \Delta\omega)] (\tau_{12} + \Delta\tau_{12})^2 - (P_{II}^0 + P_{II}^D\omega_0)\tau_{12}^2 \right\} \\ &\quad + \mu_{III} \left\{ [P_{III}^0 + P_{III}^D(\omega_0 + \Delta\omega)] (\tau_{23} + \Delta\tau_{23})^2 - (P_{III}^0 + P_{III}^D\omega_0)\tau_{23}^2 \right\} \end{aligned} \quad (41)$$

It should be noted that the incremental stress terms  $\Delta\sigma_2$ ,  $\Delta\tau_{12}$  and  $\Delta\tau_{23}$  in (40) are also dependent on incremental damage  $\Delta\omega$ . Based on the constitutive relationship (3), one has

$$\begin{aligned} \Delta\sigma_2 &= \sum_{i=1}^6 [c_{2i}^0 - c_{2i}^D(\omega_0 + \Delta\omega)] (\varepsilon_i + \Delta\varepsilon_i) - \sum_{i=1}^6 (c_{2i}^0 - c_{2i}^D\omega_0) \varepsilon_i \\ \Delta\tau_{23} &= \sum_{i=1}^6 [c_{4i}^0 - c_{4i}^D(\omega_0 + \Delta\omega)] (\varepsilon_i + \Delta\varepsilon_i) - \sum_{i=1}^6 (c_{4i}^0 - c_{4i}^D\omega_0) \varepsilon_i \\ \Delta\tau_{12} &= \sum_{i=1}^6 [c_{6i}^0 - c_{6i}^D(\omega_0 + \Delta\omega)] (\varepsilon_i + \Delta\varepsilon_i) - \sum_{i=1}^6 (c_{6i}^0 - c_{6i}^D\omega_0) \varepsilon_i \end{aligned} \quad (42)$$

where  $c_{ji}^0$  and  $c_{ji}^D$  ( $j=2,4,6$ ) are the components of  $\mathbf{C}^0$  and  $\mathbf{C}^D$  as introduced in (1).

It is obvious that (41) is a nonlinear and implicit algebraic equation of the damage increment  $\Delta\omega$ . To solve for  $\Delta\omega$  from (41), Newton's iterative method is employed with (42) incorporated in the algorithm as presented in Appendix 1.

The tangential stiffness matrix could also be obtained as given in (52) in Appendix 1 as a part of the Newton's iteration mentioned above. It is required in an implicit finite element analysis (FEA) solver, such as ABAQUS<sup>TM</sup>/Standard when a user defined material subroutine is resorted to for the

implementation of the above damage model in a structural finite element analysis. It should also be pointed out that there are many damage evolution laws in commercial software based on energy or displacement. The present model is a material model. It defines the state of damage and the evolution of the damage at a material point. In practice, the model will be applied to each integration point. Existing damage models in commercial software are different. For instance, the continuum damage model in Abaqus is defined on a plane or surface, through which decohesion is simulated, as conventionally described as cohesive zone model. Such planes or surfaces, have to be predetermined so that cohesive elements can be pre-planted

*Unloading and reloading scenarios.* It should be noted that when the material is unloaded after loading, the value of  $\Delta\omega$  becomes negative according to (37). However, damage evolution is an irreversible process, unless the material possesses self-healing function which is not available for conventional composites. Therefore, once negative value for  $\Delta\omega$  is predicted, it signifies the start of unloading process. The damage evolution should pause and the current level of damage should remain unchanged during the unloading process. An appropriate unloading criterion can be given as

$$\Delta\omega < 0 \text{ or } \eta < 1 \quad (43)$$

With the unloading process introduced, there is also the issue of reloading when the previously unloaded material is loaded up again. For such a scenario, since damage evolution process has been suspended during previous unloading process, a reloading criterion is needed to indicate that the damage evolution process is expected to resume during reloading stage. It should be the logical opposite of the unloading criterion, i.e.

$$\Delta\omega \geq 0 \text{ and } \eta \geq 1 \quad (44)$$

Unless it is satisfied, the damage state will still remain unchanged.

*Incorporation of instant failure criteria.* Apart from capturing the effects of damage growth associated with matrix cracking, the possibility of fibre failure should also be monitored. If a fibre failure mode is identified from (14), i.e., either of the ratios exceeds 1, a fibre failure is predicted. It should be noted that the fibre failure predicted here is a local failure mode. The ultimate failure of the structure like a composite laminate is characterised by the loss of load carrying capability of the structure concerned. However, any local fibre failure often appears as a close precursor to the ultimate failure in a composite structure.

## Implementation of proposed damage evolution law and its verification and validation

The damage model has been formulated under a general 3D stress condition. It is therefore applicable to problems of such nature. However, due to the availability of experimental data that can be employed as validation cases, the subsequent discussion will be specialised to a plane stress state for its applications to structures of laminated composites that can be analysed based on the classic laminate theory (CLT). As a result, the orientation of the microcracks become predetermined so that they fall into the category of so-called transverse matrix cracks. It should be also pointed out that in this paper the proposed damage model was implemented in the software MATLAB

(Mathworks, 2017) as the experimental cases adopted for model validation and verification were of macroscopically uniform stress field in each ply.

However, the proposed model could also be implemented easily in the finite element (FE) software to analyse the damage evolution in composite structures under quasi-static loading. To implement the model in this paper, the tangential stiffness matrix has been derived as presented in equation (52) in Appendix 1, which is a matrix variable required to be updated in the subroutine. To calculate the change of damage variable in a loading increment, the Newton's iterative method is employed in our model, as presented in Appendix 1, and the obtained values are also updated in the subroutine as required. With the use of subroutine, the proposed damage model will become applicable to the analysis of problems involving macroscopically non-uniform stress.

Several experimental results of glass fibre laminates were adopted for model verification and validation. Due to the limitation of test equipment, only the strain-stress curves of composite laminates were recorded in the tests, and the longitudinal stiffness degradation was derived from it for comparison with the predicted results of longitudinal stiffness properties of these composite laminates.

Among the adopted experimental results, two laminate test cases are employed to determine damage-related material property  $\mu_I$  as a first attempt. The corresponding experiments are as follows:

1. Uniaxial tensile tests on UD laminates in their transverse direction to determine the transverse tensile strength  $Y_I$  which is associated with the initiation of matrix cracking in mode I.
2. Uniaxial tensile test on cross-ply laminates of UD laminae to determine the damage-related constant  $\mu_I$  for mode I type matrix cracking damage.

### Verification with E-glass/MY750 composite laminates

*Determination of material parameters.* Experimental data obtained for the E-glass fibre  $[0/90]_s$  laminate in WWFE-I (Soden et al., 1998, 2002) were adopted to validate the proposed damage model. The particular laminate of interest consists of UD laminae, which was made of Silenka 1200tex E-glass fibre and MY750 epoxy. The corresponding UD lamina material elastic properties and strength properties as provided in (Soden et al., 1998) are summarised in Table 2 and Table 3, respectively.

In the model, the value of factor  $k$  for the coupling effects of damage between the transverse tension and in-plane shear was determined in the same manner as in (Li et al., 2019) and the obtained value is given in Table 4. In order to determine the damage-evolution-related constants  $\mu_I$  in the damage evolution law, use has been made of the experimental data obtained under uniaxial tension. In general, the stiffness reduction of the cracked lamina, i.e., the damage parameter  $\omega$ , can

**Table 2.** Material elastic properties of E-glass/MY750 UD lamina (Soden et al., 1998).

$E_1$ (MPa)	$E_2$ (MPa)	$G_{12}$ (MPa)	$\nu_{12}$	$\nu_{23}$
45600	16200	5830	0.278	0.4

**Table 3.** Strength properties of E-glass/MY750 UD lamina (Soden et al., 1998).

$X_T$ (MPa)	$X_C$ (MPa)	$Y_T$ (MPa)	$Y_C$ (MPa)	$S_L$ (MPa)
1280	800	40	145	73

**Table 4.** Damage-related and damage-evolution-related constants of E-glass/MY750 lamina.

$k$	$\mu_I$
0.310	0.98

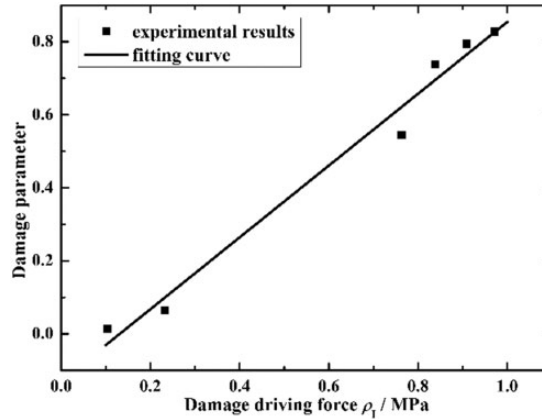


**Figure 4.** Determination of damage-evolution-related constant  $\mu_I$  based on experimental results.

be extracted from the laminate stiffness reduction based on CLT, provided that the specimens for the test are so designed that under the loading condition, there is only one lamina that is subjected to cracking damage. Similarly, the effective stress transverse to fibres in the cracked lamina could be extracted from the average stress in the laminate, given the uniaxial loading condition to the laminate, also based on CLT. The damage driving force  $\rho_I$  in the cracked laminae can be obtained from (30). Only the non-zero element  $P_I$  in  $[P]$  in (27) can be evaluated, given (28) and (29), and the value of  $\omega$ . The relationship between  $\omega$  and  $\rho_I$  directly obtained from experimental results were plotted in Figure 4 as discrete data points. Damage-evolution-related constant  $\mu_I$  was obtained as the gradient of the straight line fitted to the experimental data, as shown in Figure 4, and the obtained value is given in Table 4.

**Results and discussion.** To assess the accuracy of predictions, stress-strain curve for E-glass/MY750UD fibre cross-ply laminate under tensile loading was calculated and compared with experimental results from (Soden et al., 1998, 2002) in Figure 5. Close agreement between the predicted and the experimental stress-strain curves is apparent. Given that some of the input data were derived from the experimental results, the agreement can only serve as a necessary ‘sanity check’, an important verification.

The variation of the predicted damage variables in the  $90^\circ$  and the  $0^\circ$  plies with the applied strain has been plotted in Figure 6. As can be seen, in addition to cracking damage in the  $90^\circ$  plies, damage was also predicted in the  $0^\circ$  plies at later stage, once the transverse stress in the  $0^\circ$  plies reached transverse tensile strength and thus triggered transverse matrix cracking in the  $0^\circ$  plies. The Poisson’s effect and the constraint provided by the fibres in the  $90^\circ$  plies to the  $0^\circ$  plies were responsible for this. Specifically, as the laminate was gradually loaded, the  $0^\circ$  plies tended to shrink in the transverse direction due to Poisson’s effect. However, stiff fibres in the adjacent  $90^\circ$

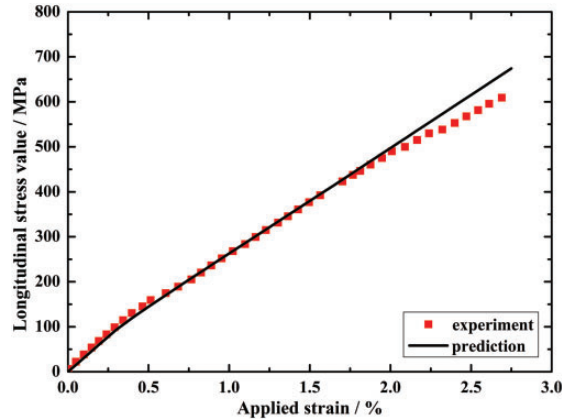


**Figure 5.** Comparison of the stress-strain curve with the experimental results for E-glass/MY750  $[0^\circ/90^\circ]_s$  laminate.

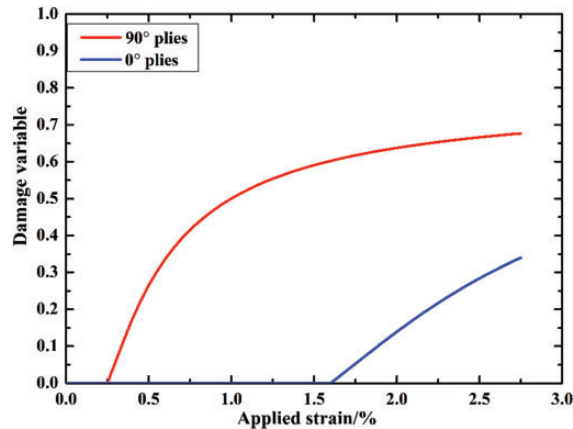


**Figure 6.** Damage parameter as function of strain in E-glass/MY750  $[0/90]_s$ .

plies tended to impede this tendency, resulting in the transverse tensile stress build up in the  $0^\circ$  plies, which eventually resulted in transverse cracking in  $0^\circ$  plies, which was sometimes described as longitudinal splitting damage in the  $0^\circ$  as reported in the cross-ply laminate specimen in (Daniels, 1945), when tensile strain exceeded 1.25%.

### *Verification and validation against E-glass/YPX3300 laminates*

In order to validate the proposed model in predicting the degradation of stiffness properties of composite laminates, experimental results of E-glass/YPX3300 cross-ply laminates as reported in (Shen et al., 2017) were employed, involving two different lay-up configurations,  $[0^\circ/90^\circ_4]_s$  and  $[0^\circ_2/90^\circ_4]_s$ . The experimental results from the former had been employed to extract the required material properties as the input to the model. Independent predictions were made to both laminates. Whilst the prediction made to the  $[0^\circ/90^\circ_4]_s$  laminate served as a necessary verification, the agreement between the prediction and the experimental data for the  $[0^\circ_2/90^\circ_4]_s$  laminate offered a meaningful case of validation. Key experimental data employed either for material property extraction or for

comparisons with the predicted results were the average stress-strain curves, from which longitudinal moduli of the laminates at different states of damage could be obtained. The obtained tangential moduli were presented graphically after being normalized with respect to the longitudinal moduli of the laminates at their undamaged states.

**Determination of material parameters.** The elastic and strength properties of E-glass/YPX3300 UD lamina are shown in Table 5 and Table 6, respectively.

The damage-related constant for E-glass/YPX3300 was determined following exactly the same procedure as described previously, utilising the experimental stress-strain curve for  $[0^\circ/90^\circ_4]_s$  laminate from (Shen, 2016). The obtained value is given in Table 7.

**Results and discussion.** Employing the obtained damage-evolution-related constants and applying the damage model to both laminates, i.e.  $[0^\circ/90^\circ_4]_s$  and  $[0^\circ_2/90^\circ_4]_s$ , the deformation and damage process in both laminates can be predicted. The results in terms of normalized longitudinal modulus are compared with the experiment data in Figure 7. The first case is in fact not truly predictive as the experimental results had been employed to extract the damage-evolution-related constant. The degree of agreement as shown in Figure 7(a) serves at least as a promising verification. The discrepancy indicates the level of error in the damage model, given various simplifications and approximations introduced in the model. In the model, both the damage representative and damage evolution model deals with transverse matrix cracking damage in composite materials, which dominates the early stage of damage evolution process. Experimental results show that the typical damage evolution process in composite materials could be divided into three main parts (Talreja and Singh, 2012). At early stage, the main damage mode is transverse matrix cracks. As the increase of loading, the matrix cracks tend to saturate and local delamination starts to emerge at the tips of matrix cracks, leading to a further degradation of stiffness properties of materials. At the later period, fibre breakage and some other diffuse damages would exist, and these damages could cause the final failure of composite structures. Since the present model only addresses the transverse matrix cracks, the influence of other damage modes is not considered, leading to the differences

**Table 5.** Material elastic properties of E-glass/YPX3300 UD lamina (Shen et al., 2017).

$E_1$ (MPa)	$E_2$ (MPa)	$G_{12}$ (MPa)	$\nu_{12}$	$\nu_{23}$
43160	10810	4850	0.306	0.3

**Table 6.** Strength properties of E-glass/YPX3300 UD lamina (Shen, 2016).

$X_T$ (MPa)	$X_C$ (MPa)	$Y_T$ (MPa)	$Y_C$ (MPa)	$S_L$ (MPa)
1114	800	38	145	66

**Table 7.** Damage- related and damage-evolution-related constants for E-glass/YPX3300 lamina.

$k$	$\mu_l$
0.314	8.5

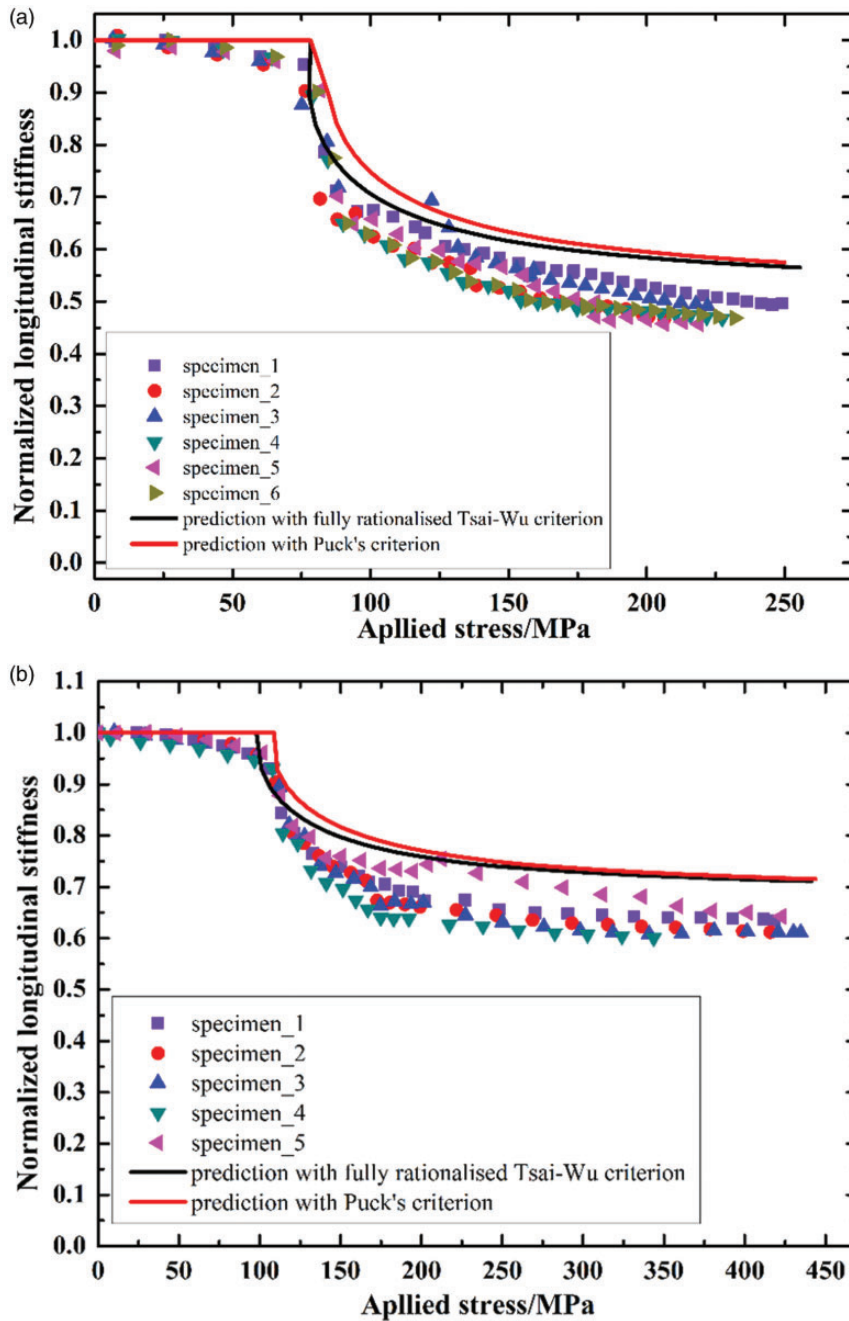


**Figure 7.** Comparison of normalized longitudinal modulus between prediction results and experimental results of E-glass/YPX3300 laminates. (a)  $[0^\circ/90^\circ_4]_s$ , (b)  $[0^\circ_2/90^\circ_4]_s$ .

between prediction and experimental results, especially when the applied stress load is large. Moreover, The proposed model also ignored the nonlinear elastic behaviour of composite materials under quasi-static loadings. Experimental results show that the longitudinal modulus of composite laminates start to decrease due to the tensile nonlinearity before the initiation of matrix cracks (Shen et al., 2017), but this effect is not included in our present model, leading to the differences between the prediction results and experimental results. Given the complex nature of the damage problem, the error should fall in an acceptable range for engineering applications.

The results as presented in Figure 7(b) should be considered true predictions in a sense that the experimental results for this case had not been employed directly or indirectly. The agreement with experimental data is certainly satisfactory, at least no worse than that in Figure 7(a).

Note that there are two curves shown in Figure 7(a) and (b). One in black corresponds to the damage model where damage onset is predicted with the rationalised Tsai-Wu criterion, while for red curve, damage initiation was predicted based on the Puck criterion, as was originally used in (Yu, 2016). No significant differences have been observed. However, recent efforts on the full rationalisation of the Tsai-Wu criterion (Li et al., 2022a, 2022b) rendered the formulation free from any fudge factors and it is also much simpler to implement than the Puck criterion. The identification of failure modes can be satisfactorily accommodated by adopting the mode identification scheme based on the rationalised maximum stress criterion (Li, 2020) as described in sub-section ‘Damage initiation criterion’ previously.

### Model verification with fiberite/HyE 9082Af composite laminates

Apart from the verification in predicting the stiffness degradation of cross-ply laminates, experimental results in (Joffe and Varna, 1999) were also adopted to validate the proposed model in predicting the stiffness degradation of composite laminates with off-axis plies. In their experiments, the specimen was made from Fiberite/HyE 9082Af, and the configuration of laminates was  $[\pm\theta/90^{\circ}_4]_s$  with  $\theta = 0^{\circ}, 15^{\circ}, 30^{\circ}$  and  $40^{\circ}$ .

*Determination of material parameters.* The basic elastic properties and strength properties of Fiberite/HyE 9082Af UD lamina are shown in Table 8 and Table 9, respectively (Joffe and Varna, 1999; Moure et al., 2014). Out of the four laminates, the experimental results from the  $[30^{\circ}_2/90^{\circ}_4]_s$  laminate were employed to extract the damage-evolution-related constant of this type of composite and the obtained value are listed in Table 10. The comparison with the experimental results obtained from the remaining three laminates would serve as validation cases.

**Table 8.** Material elastic properties of Fiberite/HyE 9082Af UD lamina (Joffe and Varna, 1999).

$E_1$ (MPa)	$E_2$ (MPa)	$G_{12}$ (MPa)	$\nu_{12}$	$\nu_{23}$
44730	12760	5800	0.297	0.42

**Table 9.** Strength properties of Fiberite/HyE 9082Af UD lamina (Moure et al., 2014).

$X_T$ (MPa)	$X_C$ (MPa)	$Y_T$ (MPa)	$Y_C$ (MPa)	$S_L$ (MPa)
1020	620	40	140	60

**Table 10.** Damage-related and damage-evolution-related constants of Fiberite/HyE 9082Af lamina.

$k$	$\mu_l$
0.329	3.5

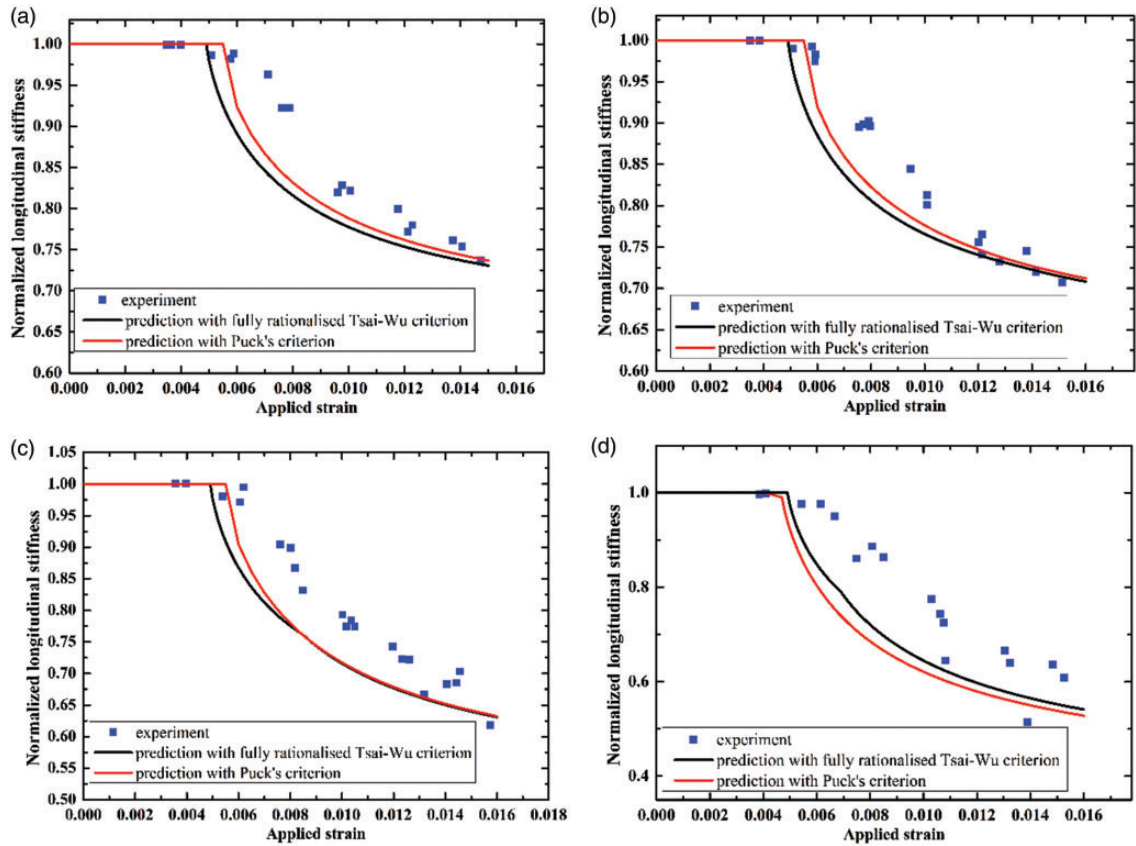


**Figure 8.** Comparison of normalized longitudinal modulus between prediction results and experimental results of Fiberite/HyE 9082Af laminates. (a)  $[0^\circ_2/90^\circ_4]_s$ , (b)  $[15^\circ_2/90^\circ_4]_s$ , (c)  $[30^\circ_2/90^\circ_4]_s$ , and (d)  $[40^\circ_2/90^\circ_4]_s$ .

**Results and discussion.** The comparisons between the predictions and experimental results are shown in Figure 8 in terms of the degradation of the normalized longitudinal modulus. Out of the four laminates corresponding to Figure 8(a) and (d), the case for Figure 8(c) should be considered as a verification, as it is meant to reproduce the test case from which the input data were extracted. It is a laminate with off-axis plies. Under uniaxial tension, an in-plane along-fibre shear stress is generated. Any discrepancy between the prediction and the experimental data gives a good indication of possible errors in the model due to the assumptions and approximations employed. The agreements as shown in the remaining three cases in Figure 8(a), (b) and (d), respectively, for laminates of different layups are valid cases of validation of the model.

The predicted results of stiffness degradation of composite laminates with off-axis plies as shown in Figure 8 are generally in good agreement with experimental results, indicating the capability of proposed model in predicting stiffness degradation of both cross-ply laminates and laminates with off-axis plies due to transverse matrix cracking damage under quasi-static loading.

It should be noted that the in-plane shear nonlinearity in presence of off-axis plies in the laminate makes the problem significantly more complicated if the interactions between this nonlinearity and that caused by damage are considered (Li et al., 2005). A consistent approach of incorporating along-fibre shear nonlinearity under a general 3D stress state has been formulated in (Li et al., 2021). Whilst it is of interest to incorporate such interactions in the new damage model, it is beyond the scope of this paper and will be pursued as a future development. A significant part of the disparity between the predicted results and the experimental data can be attributed to this consideration. In addition, the neglect of other damage modes, e.g., local delamination at crack tips at increasing loading would lead to the further errors between the prediction results and experimental results, as discussed in part of sub-section 'Verification and validation against E-glass/YPX3300 laminates'.

Again, predictions using the Puck criterion for damage initiation have also been included in Figure 8. They remain comparable with the present results.

## **Conclusion**

In this paper, a new damage evolution model is formulated based on the concept of damage driving force to predict the initiation and evolution of transverse matrix cracks in composite materials under quasi-static loading. The expression of the damage driving force can be presented in a decoupled form with each component corresponding to a mode resembling one of the three well-known modes of fracture. At the implementation level, the Newton's iterative method has been derived to deal with the nonlinearity involved in the problem. This damage evolution law is formulated at macro scale, although it is to model the effects of micro cracks in the composite. First attempt has been made to incorporate the fully rationalised Tsai-Wu failure criterion (Li et al., 2022) to predict the damage initiation and the fully rationalised maximum stress criterion (Li, 2020) to predict the damage modes in the composite. The newly formulated damage evolution model takes account of unloading and reloading based on appropriately proposed criteria for these processes respectively to duly reflect the irreversible nature of damage. Hence the model could be used to predict the deformation of composite structures involving damage initiation and evolution when the structure is under complex loading conditions. With the help of classical laminate theory, it can also be applied to laminates of arbitrary layups although for the examples in the present paper only one of them has been used. The application of the new model requires only three newly defined damage-evolution-related material properties that can be extracted from a set of appropriate tests on a simple laminate layup before the model can be applied to laminates of arbitrary layups under arbitrarily loading cases.

Several sets of the experimental results for glass fibre reinforced composite laminates were adopted for the verification and validation of new model, including the stress-strain curves and stiffness reduction as a function of the applied load. Good agreements have been observed in general.

It should be pointed out that due to the neglect of nonlinear elastic behaviour of composite materials, the proposed model cannot deal with damage behaviour of composite materials involving significant nonlinearity, and this would be addressed in the further work. Besides, both the damage representative model and damage evolution model in the present model deal with transverse cracking damage only in uniaxially fibre reinforced composites, which dominates the early stage of damage evolution process. The evolution of some other damage modes, for instance, local

delamination and fibre breakage, are not considered. These damages often initiate and develop after the saturation of transverse matrix cracks and would lead to the final failure of composite structures. Hence, the present model is only limited to transverse cracking damages and cannot analyse further damage and failure behaviour of composite materials after the saturation of transverse cracking damage. Considering the difference between fatigue loading and quasi-static loading, the proposed damage evolution model is only valid for predicting the evolution of transverse matrix cracks in composite materials under quasi-static loadings, and it cannot predict the matrix cracks initiation and evolution in composite materials under fatigue loading.

### Declaration of conflicting interests

The author(s) declared no potential conflicts of interest with respect to the research, authorship, and/or publication of this article.

### Funding

The author(s) disclosed receipt of the following financial support for the research, authorship, and/or publication of this article: The financial support from AECC Commercial Aircraft Engine, Co. Ltd., China, through Grant No. RGS 106619 (from July 2012 to July 2015), is gratefully acknowledged.

### ORCID iD

Wenxuan Qi  <https://orcid.org/0000-0002-9701-5625>

### References

- Abdullah NA, Curiel-Sosa JL, Taylor ZA, et al. (2017) Transversal crack and delamination of laminates using XFEM. *Composite Structures* 173: 78–85.
- Allix O and Hild F (2002) *Continuum Damage Mechanics of Materials and Structures*. Amsterdam: Elsevier.
- Anderson TL (2017) *Fracture Mechanics: Fundamentals and Applications*. Boca Raton: CRC Press.
- Babaei R and Farrokhabadi A (2017) A computational continuum damage mechanics model for predicting transverse cracking and splitting evolution in open hole cross-ply composite laminates. *Fatigue & Fracture of Engineering Materials & Structures* 40(3): 375–390.
- Braun M and Ariza MP (2020) A progressive damage based lattice model for dynamic fracture of composite materials. *Composites Science and Technology* 200: 108335.
- Braun M, Iváñez I and Ariza MP (2021) A numerical study of progressive damage in unidirectional composite materials using a 2D lattice model. *Engineering Fracture Mechanics* 249: 107767.
- Braun M, Iváñez I and Ariza MP (2024) A discrete lattice model with axial and angular springs for modeling fracture in fiber-reinforced composite laminates. *European Journal of Mechanics – A/Solids* 104: 105213.
- Daghia F and Ladeveze P (2013) Identification and validation of an enhanced mesomodel for laminated composites within the WWFE-III. *Journal of Composite Materials* 47(20-21): 2675–2693.
- Daniels HE (1945) The statistical theory of the strength of bundles of threads. *I. Proc R Soc Lond A Math Phys Sci* 183: 405–435.
- Dimitri R, Fantuzzi N, Li Y, et al. (2017) Numerical computation of the crack development and SIF in composite materials with XFEM and SFEM. *Composite Structures* 160: 468–490.
- Echaabi J, Trochu F and Gauvin R (1996) Review of failure criteria of fibrous composite materials. *Polymer Composites* 17(6): 786–798.
- Edge EC (1998) Stress-based Grant–Sanders method for predicting failure of composite laminates. *Composites Science and Technology* 58(7): 1033–1041.
- Galadima YK, Oterkus S, Oterkus E, et al. (2023) A nonlocal method to compute effective properties of viscoelastic composite materials based on peridynamic computational homogenization theory. *Composite Structures* 319: 117147.

- Gupta AK, Patel BP and Nath Y (2012) Continuum damage mechanics approach to composite laminated shallow cylindrical/conical panels under static loading. *Composite Structures* 94(5): 1703–1713.
- Shen H (2016) *Synergistic Damage Mechanics for Multi-Directional Properties of Composite Laminates with Experimental Verification*. Nanjing: Nanjing University of Aeronautics and Astronautics.
- Haque BZ (2015) A progressive composite damage model for unidirectional and woven fabric composites. *MAT162 User Manual* 10. University of Delaware: Delaware, USA.
- Hinton MJ, Kaddour AS and Soden PD (2002) A comparison of the predictive capabilities of current failure theories for composite laminates, judged against experimental evidence. *Composites Science and Technology* 62(12–13): 1725–1797.
- Hinton MJ, Kaddour AS and Soden PD (2004) A further assessment of the predictive capabilities of current failure theories for composite laminates: comparison with experimental evidence. *Composites Science and Technology* 64(3–4): 549–588.
- Jain JR and Ghosh S (2009) Damage evolution in composites with a homogenization-based continuum damage mechanics model. *International Journal of Damage Mechanics* 18(6): 533–568.
- Joffé R and Varna J (1999) Analytical modeling of stiffness reduction in symmetric and balanced laminates due to cracks in 90° layers. *Composites Science and Technology* 59(11): 1641–1652.
- Kaddour AS and Hinton MJ (2012) Benchmarking of triaxial failure criteria for composite laminates: Comparison between models of “part (a)” of “WWFE-II. *Journal of Composite Materials* 46(19-20): 2595–2634.
- Kaddour AS and Hinton MJ (2013) Maturity of 3D failure criteria for fibre-reinforced composites: Comparison between theories and experiments: Part B of WWFE-II. *Journal of Composite Materials* 47(6–7): 925–966.
- Kaddour AS, Hinton MJ, Smith PA, et al. (2013a) A comparison between the predictive capability of matrix cracking, damage and failure criteria for fibre reinforced composite laminates: Part a of the third world-wide failure exercise. *Journal of Composite Materials* 47(20–21): 2749–2779.
- Kaddour AS, Hinton MJ, Smith PA, et al. (2013b) The background to the third world-wide failure exercise. *Journal of Composite Materials* 47(20–21): 2417–2426.
- Kaddour AS, Hinton MJ and Soden PD (2004) A comparison of the predictive capabilities of current failure theories for composite laminates: additional contributions. *Composites Science and Technology* 64(3–4): 449–476.
- Knops M (2008) *Analysis of Failure in Fiber Polymer Laminates: The Theory of Alfred Puck*. Berlin: Springer Science & Business Media.
- Knops M and Bögle C (2006) Gradual failure in fibre/polymer laminates. *Composites Science and Technology* 66(5): 616–625.
- Li S (2020) The maximum stress failure criterion and the maximum strain failure criterion: Their unification and rationalization. *Journal of Composites Science* 4(4): 157.
- Li S, Reid SR and Soden PD (1998) A continuum damage model for transverse matrix cracking in laminated fibre-reinforced composites. *Philosophical Transactions of the Royal Society of London Series A: Mathematical, Physical and Engineering Sciences* 356(1746): 2379–2412.
- Li S, Reid SR, Soden PD, et al. (2005) Modelling transverse cracking damage in thin, filament-wound tubes subjected to lateral indentation followed by internal pressure. *International Journal of Mechanical Sciences* 47(4–5): 621–646.
- Li S, Xu M and Sitnikova E (2022b) The formulation of the quadratic failure criterion for transversely isotropic materials: Mathematical and logical considerations. *Journal of Composites Science* 6(3): 82.
- Li S, Xu M and Sitnikova E (2022a) Fully rationalised Tsai-Wu failure criterion for transversely isotropic materials. In: Tsai S (ed.) *Double-Double – A New Perspective in Manufacture and Design of Composites*. Stanford: JEC & Stanford, pp. 173–206.
- Li S, Xu M, Yan S, et al. (2021) On the objectivity of the nonlinear along-fibre shear stress–strain relationship for unidirectionally fibre-reinforced composites. *Journal of Engineering Mathematics* 127(1): 1–13.
- Li F, Yang X, Gao W, et al. (2023) A single-layer peridynamic model for failure analysis of composite laminates. *Materials Today Communications* 37: 106988.

- Li S, Wang M, Jeanmeure L, et al. (2019) Damage related material constants in continuum damage mechanics for unidirectional composites with matrix cracks. *International Journal of Damage Mechanics* 28(5): 690–707.
- LS-DYNA (2015) *Keyword User's Manual, Material Models*. ANSYS: Pennsylvania, US.
- Maplesoft (2014). *Maple User Manual*. Maple: Waterloo, Canada.
- Matzenmiller A, Lubliner J and Taylor RL (1995) A constitutive model for anisotropic damage in fiber-composites. *Mechanics of Materials* 20(2): 125–152.
- Mohammadi B, Olia H and Hosseini-Toudeshky H (2015) Intra and damage analysis of laminated composites using coupled continuum damage mechanics with cohesive interface layer. *Composite Structures* 120: 519–530.
- Moure MM, Sanchez-Saez S, Barbero E, et al. (2014) Analysis of damage localization in composite laminates using a discrete damage model. *Composites Part B: Engineering* 66: 224–232.
- Mukhopadhyay S and Hallett SR (2019) A directed continuum damage mechanics method for modelling composite matrix cracks. *Composites Science and Technology* 176: 1–8.
- Murakami S (2012) *Continuum Damage Mechanics: A Continuum Mechanics Approach to the Analysis of Damage and Fracture*. Berlin: Springer Science & Business Media.
- Ni T, Zaccariotto M and Galvanetto U (2023) A peridynamic approach to simulating fatigue crack propagation in composite materials. *Philosophical Transactions. Series A, Mathematical, Physical, and Engineering Sciences* 381(2240): 20210217.
- Onodera S and Okabe T (2020) Analytical model for determining effective stiffness and mechanical behavior of polymer matrix composite laminates using continuum damage mechanics. *International Journal of Damage Mechanics* 29(10): 1512–1542.
- Puck A and Schürmann H (2002) Failure analysis of frp laminates by means of physically based phenomenological models. *Composites Science and Technology* 62(12–13): 1633–1662.
- Mathworks (2017) *Matlab R2017a*. Natick, MA, USA.
- Salavatian M and Smith L V (2015) An investigation of matrix damage in composite laminates using continuum damage mechanics. *Composite Structures* 131: 565–573.
- Sapozhnikov SB and Cheremnykh SI (2013) The strength of fibre reinforced polymer under a complex loading. *Journal of Composite Materials* 47(20–21): 2525–2552.
- Shen H, Yao W, Qi W, et al. (2017) Experimental investigation on damage evolution in cross-ply laminates subjected to quasi-static and fatigue loading. *Composites Part B: Engineering* 120: 10–26.
- Soden PD, Hinton MJ and Kaddour AS (1998) A comparison of the predictive capabilities of current failure theories for composite laminates. *Composites Science and Technology* 58(7): 1225–1254.
- Soden PD, Hinton MJ and Kaddour AS (1998) Lamina properties, lay-up configurations and loading conditions for a range of fibre-reinforced composite laminates. *Composites Science and Technology* 58(7): 1011–1022.
- Soden PD, Hinton MJ and Kaddour AS (2002) Biaxial test results for strength and deformation of a range of E-glass and carbon fibre reinforced composite laminates: Failure exercise benchmark data. *Composites Science and Technology* 62(12–13): 1489–1514.
- Soden PD, Kaddour AS and Hinton MJ (2004) Recommendations for designers and researchers resulting from the world-wide failure exercise. *Composites Science and Technology* 64(3-4): 589–604.
- Sun M, Liu L, Mei H, et al. (2023) A bond-based peridynamic model with matrix plasticity for impact damage analysis of composite materials. *Materials* 16(7): 2884.
- Swati RF, Wen LH, Elahi H, et al. (2019) Extended finite element method (XFEM) analysis of fiber reinforced composites for prediction of micro-crack propagation and delaminations in progressive damage: A review. *Microsystem Technologies* 25(3): 747–763.
- Talreja R (1985) A continuum mechanics characterization of damage in composite materials. *Proceedings of the Royal Society of London A Mathematical and Physical Sciences* 399: 195–216.
- Talreja R (1987) Internal variable damage mechanics of composite materials. *Yielding, Damage, and Failure of Anisotropic Solids*: 509–533.
- Talreja R and Singh CV (2012) *Damage and Failure of Composite Materials*. Cambridge: Cambridge University Press.

- Tao Y, Chen H, Yao K, et al. (2017) Experimental and theoretical studies on inter-fiber failure of unidirectional polymer-matrix composites under different strain rates. *International Journal of Solids and Structures* 113–114: 37–46.
- Thollon Y and Hochard C (2009) A general damage model for woven fabric composite laminates up to first failure. *Mechanics of Materials* 41(7): 820–827.
- Yu T (2016) *Continuum Damage Mechanics Models and Their Applications to Composite Components of Aero-Engines*. Nottingham: The University of Nottingham.
- Wang L, Zheng C, Luo H, et al. (2015) Continuum damage modeling and progressive failure analysis of carbon fiber/epoxy composite pressure vessel. *Composite Structures* 134: 475–482.
- Williams K V, Vaziri R and Poursartip A (2003) A physically based continuum damage mechanics model for thin laminated composite structures. *International Journal of Solids and Structures* 40(9): 2267–2300.
- Zhong S, Guo L, Liu G, et al. (2015) A continuum damage model for three-dimensional woven composites and finite element implementation. *Composite Structures* 128: 1–9.
- Zinoviev PA, Grigoriev S v, Lebedeva O v, et al. (1998) The strength of multilayered composites under a plane-stress state. *Composites Science and Technology* 58(7): 1209–1223.

## Appendix I

To calculate the increment of damage parameter  $\Delta\omega$  from (41) with relevant stress increments as given in (42), Newton's iterative method can be employed as shown below. To facilitate this, rearrange (41) to introduce a new function as follows.

$$\begin{aligned}
 f(\Delta\omega) = & \Delta\omega - \mu_I \left\{ [P_I^0 + P_I^D(\omega_0 + \Delta\omega)](\sigma_2 + \Delta\sigma_2)^2 - (P_I^0 + P_I^D\omega_0)\sigma_2^2 \right\} \\
 & - \mu_{II} \left\{ [P_{II}^0 + P_{II}^D(\omega_0 + \Delta\omega)](\tau_{12} + \Delta\tau_{12})^2 - (P_{II}^0 + P_{II}^D\omega_0)\tau_{12}^2 \right\} \\
 & - \mu_{III} \left\{ [P_{III}^0 + P_{III}^D(\omega_0 + \Delta\omega)](\tau_{23} + \Delta\tau_{23})^2 - (P_{III}^0 + P_{III}^D\omega_0)\tau_{23}^2 \right\}
 \end{aligned} \quad (45)$$

Solving (38) is equivalent to finding an appropriate value for  $\Delta\omega$  which makes  $f(\Delta\omega) = 0$ . Newton's iteration scheme can be employed to find the root for such a homogeneous equation through the following formula:

$$\Delta\omega_k = \Delta\omega_{k-1} + \delta_k \quad \text{for the } k\text{-th iteration} \quad (46)$$

with  $\Delta\omega_0 = 0$ , and

$$\delta_k = -\frac{f(\Delta\omega_{k-1})}{f'(\Delta\omega_{k-1})} \quad (47)$$

where

$$\begin{aligned}
 f'(\Delta\omega) = & 1 - \mu_I(\sigma_2 + \Delta\sigma_2) \left\{ P_I^D(\sigma_2 + \Delta\sigma_2) + 2[P_I^0 + P_I^D(\omega_0 + \Delta\omega)] \frac{\partial \Delta\sigma_2}{\partial \Delta\omega} \right\} \\
 & - \mu_{II}(\tau_{12} + \Delta\tau_{12}) \left\{ P_{II}^D(\tau_{12} + \Delta\tau_{12}) + 2[P_{II}^0 + P_{II}^D(\omega_0 + \Delta\omega)] \frac{\partial \Delta\tau_{12}}{\partial \Delta\omega} \right\} \\
 & - \mu_{III}(\tau_{23} + \Delta\tau_{23}) \left\{ P_{III}^D(\tau_{23} + \Delta\tau_{23}) + 2[P_{III}^0 + P_{III}^D(\omega_0 + \Delta\omega)] \frac{\partial \Delta\tau_{23}}{\partial \Delta\omega} \right\}
 \end{aligned} \quad (48)$$

whilst

$$\begin{aligned}\frac{\partial \Delta \sigma_2}{\partial \Delta \omega} &= - \sum_{i=1}^6 c_{2i}^D (\varepsilon_i + \Delta \varepsilon_i) \\ \frac{\partial \Delta \tau_{23}}{\partial \Delta \omega} &= - \sum_{i=1}^6 c_{4i}^D (\varepsilon_i + \Delta \varepsilon_i) \\ \frac{\partial \Delta \tau_{12}}{\partial \Delta \omega} &= - \sum_{i=1}^6 c_{6i}^D (\varepsilon_i + \Delta \varepsilon_i)\end{aligned}\quad (49)$$

with  $c_{ij}^D$  as given in (2).

When the above defined iterations converge,  $\Delta \omega_k$  converges to  $\Delta \omega$ . It should be used to update the damage state. As a result, the stress state and the tangential stiffness matrix of damaged material incorporating evolving damage variable can be determined at a given deformation state  $(\varepsilon + \Delta \varepsilon)$ . According to stress-strain relationship as given in (3), its incremental form can be obtained in a straightforward manner, from which the current stress state can be obtained as follows, where boldface letters are employed to stand for tensor for the neatness of the expressions involved.

$$\begin{aligned}\Delta \boldsymbol{\sigma} &= \left( \mathbf{C}^0 + \mathbf{C}^D(\omega_0 + \Delta \omega) \right) (\boldsymbol{\varepsilon} + \Delta \boldsymbol{\varepsilon}) - (\mathbf{C}^0 + \mathbf{C}^D \omega_0) \boldsymbol{\varepsilon} \\ &= (\mathbf{C}^0 + \mathbf{C}^D \omega_0) \Delta \boldsymbol{\varepsilon} + \mathbf{C}^D (\boldsymbol{\varepsilon} + \Delta \boldsymbol{\varepsilon}) \Delta \omega\end{aligned}\quad (50)$$

Differentiate the above with respect to  $\Delta \boldsymbol{\varepsilon}$ , one obtains

$$\begin{aligned}\mathbf{C}_t &= \frac{\partial \Delta \boldsymbol{\sigma}}{\partial \Delta \boldsymbol{\varepsilon}} = \mathbf{C}^0 + \mathbf{C}^D(\omega_0 + \Delta \omega) + \mathbf{C}^D (\boldsymbol{\varepsilon} + \Delta \boldsymbol{\varepsilon}) \frac{\partial \Delta \omega}{\partial \Delta \boldsymbol{\varepsilon}} \\ &= \mathbf{C}^0 + \mathbf{C}^D(\omega_0 + \Delta \omega) + \mathbf{C}^D (\boldsymbol{\varepsilon} + \Delta \boldsymbol{\varepsilon}) \frac{\partial \Delta \omega}{\partial \boldsymbol{\sigma}} \frac{\partial \Delta \boldsymbol{\sigma}}{\partial \Delta \boldsymbol{\varepsilon}} \\ &= \mathbf{C}^0 + \mathbf{C}^D(\omega_0 + \Delta \omega) + \mathbf{C}^D (\boldsymbol{\varepsilon} + \Delta \boldsymbol{\varepsilon}) \frac{\partial \Delta \omega}{\partial \Delta \boldsymbol{\sigma}} \mathbf{C}_t\end{aligned}\quad (51)$$

The tangential stiffness  $[\mathbf{C}_t]$  can then be obtained after an appropriate rearrangement of the above

$$\mathbf{C}_t = \left( \mathbf{I} - \mathbf{C}^D (\boldsymbol{\varepsilon} + \Delta \boldsymbol{\varepsilon}) \frac{\partial \Delta \omega}{\partial \Delta \boldsymbol{\sigma}} \right)^{-1} \left( \mathbf{C}^0 + \mathbf{C}^D(\omega_0 + \Delta \omega) \right)\quad (52)$$

where  $[\mathbf{I}]$  is identity matrix and  $\frac{\partial \Delta \omega}{\partial \Delta \boldsymbol{\sigma}}$  can be obtained using (41) as follows.

$$\begin{aligned}\frac{\partial \Delta \omega}{\partial \Delta \boldsymbol{\sigma}} &= \left[ \begin{array}{cccccc} \frac{\partial \Delta \omega}{\partial \Delta \sigma_1} & \frac{\partial \Delta \omega}{\partial \Delta \sigma_2} & \frac{\partial \Delta \omega}{\partial \Delta \sigma_3} & \frac{\partial \Delta \omega}{\partial \Delta \tau_{12}} & \frac{\partial \Delta \omega}{\partial \Delta \tau_{13}} & \frac{\partial \Delta \omega}{\partial \Delta \tau_{23}} \\ \frac{\partial}{\partial} & \frac{\partial}{\partial} & \frac{\partial}{\partial} & \frac{\partial}{\partial} & \frac{\partial}{\partial} & \frac{\partial}{\partial} \end{array} \right] \mathbf{Q}\end{aligned}\quad (53)$$

where

$$Q = \mu_I \left( P_I^0 + P_I^D(\omega^0 + \Delta\omega) \right) \cdot (\sigma_2^0 + \Delta\sigma_2)^2 + \mu_{II} \left( P_{II}^0 + P_{II}^D(\omega^0 + \Delta\omega) \right) \cdot (\tau_{12}^0 + \Delta\tau_{12})^2 + \mu_{III} \left( P_{III}^0 + P_{III}^D(\omega^0 + \Delta\omega) \right) \cdot (\tau_{23}^0 + \Delta\tau_{23})^2 \quad (54)$$

with the expressions of  $P_I^0$ ,  $P_{II}^0$ ,  $P_{III}^0$ ,  $P_I^D$ ,  $P_{II}^D$  and  $P_{III}^D$  as given in (29). Equation (53) can be manipulated into

$$\frac{\partial \Delta\omega}{\partial \Delta\sigma} = Q_\omega \frac{\partial \Delta\omega}{\partial \Delta\sigma} + [0 \quad Q_I \quad 0 \quad Q_{II} \quad 0 \quad Q_{III}] \quad (55)$$

where

$$Q_\omega = \mu_I P_I^D (\sigma_2^0 + \Delta\sigma_2)^2 + \mu_{II} P_{II}^D (\tau_{12}^0 + \Delta\tau_{12})^2 + \mu_{III} P_{III}^D (\tau_{23}^0 + \Delta\tau_{23})^2$$

$$Q_I = 2\mu_I \left( P_I^0 + P_I^D(\omega^0 + \Delta\omega) \right) (\sigma_2^0 + \Delta\sigma_2)$$

$$Q_{II} = 2\mu_{II} \left( P_{II}^0 + P_{II}^D(\omega^0 + \Delta\omega) \right) (\tau_{12}^0 + \Delta\tau_{12})$$

$$Q_{III} = 2\mu_{III} \left( P_{III}^0 + P_{III}^D(\omega^0 + \Delta\omega) \right) (\tau_{23}^0 + \Delta\tau_{23})$$

Re-arranging (55), one obtains

$$\frac{\partial \Delta\omega}{\partial \Delta\sigma} = \frac{1}{1 - Q_\omega} [0 \quad Q_I \quad 0 \quad Q_{II} \quad 0 \quad Q_{III}] \quad (56)$$

With this, the evaluation of the tangential stiffness as given in (51) can be fulfilled.